Journal of Environmental Management 394 (2025) 127289

Contents lists available at ScienceDirect

Journal of Environmental Management

journal homepage: www.elsevier.com/locate/jenvman

Research article

Advanced TiO_2-based catalysts for polypropylene degradation in aquatic media

A. Egea-Corbacho [a,b], A.P. Martín-García [a,*], J.M. Salas-Calvo [a], D. Coello [a,b], R. Rodríguez [a,c], I. Moreno-Garrido [d], M. Sendra [d], M.P. Yeste [e,f]

[a] Department of Environmental Technologies, Faculty of Marine and Environmental Sciences, University of Cadiz, Puerto Real, 11510, Cádiz, Spain
[b] INMAR-Marine Research Institute, CEIMAR International Campus of Excellence of the Sea, University of Cadiz, Puerto Real, Cadiz, Spain
[c] IVAGRO-Wine and Agrifood Research Institute, University of Cadiz, Puerto Real, 11510, Cádiz, Spain
[d] Department of Ecology and Coastal Management, Institute of Marine Sciences of Andalusia (ICMAN-CSIC), Campus Río San Pedro, Puerto Real, 11510, Cádiz, Spain
[e] Department of Materials Science and Metallurgical Engineering and Inorganic Chemistry, Universidad de Cádiz, Puerto Real, 11510, Spain
[f] Instituto de Microscopía Electrónica y Materiales (IMEYMAT), Universidad de Cadiz, Puerto Real, 11510, Spain

ARTICLE INFO

Keywords:
Wastewater
Photocatalysis
Advanced oxidation processes (AOPs)
Polymer degradation
Environmental remediation

ABSTRACT

Plastics are polluting our environment and oceans with a large number and variety of organic and inorganic compounds that arise as a consequence of the current industrial development. Every year we release to the environment millions of tons of plastics whose total elimination may take centuries. The exponential increase in the production of this material is causing a serious environmental problem, resulting in the generation of a large amount of this waste. Microplastics (MPs) are released into the environment in different ways, but one of the most important is through effluents from wastewater treatment plants, since no specific method is used to eliminate or degrade these MPs before they are discharged into the environment. Polypropylene (PP), together with low-density polyethylene (PE), are the most common MPs found in the environment, being released in an amount of approximately 112 million tons per year. Three catalysts, ZnO/TiO_2, CeO_2/TiO_2 and $ZnO\text{-}CeO_2/TiO_2$, were synthesized using the incipient wetness impregnation technique and tested under UV-A and UV-B irradiation for the degradation of polypropylene (PP) particles. A degradation of 6.6 ± 1.6 % of MP area in wastewater was obtained, slightly lower than the 8.4 ± 1.0 % observed with ultrapure water, likely due to the presence of organic matter and other compounds in the Waste Water Treatment Plant (WWTP) outlet. Additionally, toxicity assays using *Phaeodactylum tricornutum* revealed significant differences among treatments. The $ZnO\text{-}CeO_2/TiO_2$ catalyst resulted in lower growth inhibition compared to ZnO/TiO_2, which showed toxicity levels similar to those of UV-aged PP-MPs without catalyst, highlighting the role of catalyst composition in modulating the environmental toxicity of degraded microplastics.

1. Introduction

Plastics are synthetic materials prepared from organic polymers. The most commonly used polymers are poly styrene (PE), polypropylene (PP), polyvinyl chloride (PVC) and polyethylene terephthalate (PET), which are generally treated with chemical additives to transform them into useful plastics (Wagner and Lambert, 2018). They are characterized by attractive properties, which allow them to mold objects of various shapes and sizes. These properties are moisture, light and temperature resistance, in addition to durability, high flexibility, corrosion resistance, high strength-to-weight ratio, low costs and ease of manufacturing (Da Costa et al., 2018). MPs are synthetic organic polymer particles that are less than 5 mm in size and have a minimum size of 1 μm (Bayo et al., 2020).

MPs remain for a long time in environments due to their high durability, stability, small size and lightweight. Precisely because of their small size, they are ingested by aquatic organisms and may cause harmful effects, eventually ending up in food and water for human consumption (Zhu et al., 2018). The hydrophobic nature and relatively large surface area/volume ratio of MPs cause the adsorption of numerous toxic pollutants, such as polychlorinated biphenyls (PCBs), polycyclic aromatic hydrocarbons (PAHs), polybrominated diphenyl

* Corresponding author.
E-mail address: ana.martingarcia@uca.es (A.P. Martín-García).

https://doi.org/10.1016/j.jenvman.2025.127289
Received 20 June 2025; Received in revised form 16 August 2025; Accepted 7 September 2025
Available online 19 September 2025

ethers (PBDEs), dichlorodiphenyltrichloroethane (DDT), endocrine disrupting compounds (EDCs), various pharmaceuticals and metals (Reddy et al., 2018) . Regarding metals, PP shows higher heavy metal adsorption capacity compared to other polymers. With this, we can observe that MPs are an important vector for the transport of heavy metals in both marine waters and freshwater, causing harmful damage to humans and aquatic animals (Selvam et al., 2021).

MPs have been identified in about 220 types of aquatic animals such as mussels, crabs, seabirds, and oysters (Jinhui et al., 2019). The hazards of ingestion of MPs include growth impairment and physical deterioration (Jovanović, 2017). MPs can be present in a wide range of foods and beverages and approximately 6292 ± 10,521 MP/L > 1 μm have been detected in bottled waters. PP is the dominant plastic in the environment, contributing 27 % of total plastic loss. By environmental PE, 42 %, 41 %, and 14 % accumulated in the ocean, soil, and freshwater, respectively (Schymansk et al., 2018). Wastewater treatment plants (WWTPs) play a key role in the removal of MP particles before these waters are discharged to the environment. These have a high efficiency as they capture between 88 and 99.9 % of the load of MPs of size >20 μm. A large concentration is observed in the influent stream of WWTPs, most of which is trapped in the sludge; however, studies have shown that between 0.1 % and 12 % of detectable size (i.e., >20 μm) MPs are still released to the environment via the effluent. In general, the concentration of effluent MPs is several orders of magnitude lower than the concentrations in the influent. It is estimated that 2.5 billion MPs particles are released through this WWTP effluent to the environment every month (Uddin et al., 2020).

Due to this concern, it is essential to identify technologies for the remediation of MPs in the aquatic environment. Advanced Oxidation Processes (AOPs) are a promising alternative for the solution of environmental problems. Among the AOPs is photocatalysis. Zinc oxide (ZnO) is considered very suitable for the degradation of commercial MPs as it has the ability to absorb visible light, due to significant electron movement and low toxicity to human and marine life (Uheida et al., 2021). Cerium dioxide (CeO_2) is an alternative photocatalyst under UV light irradiation for the degradation of MPs due to its versatility, cost-effectiveness, non-toxicity, and physical and chemical stability (Zhao et al., 2007).

Titanium dioxide (TiO_2) is recognized as a highly effective photocatalyst because it has several beneficial properties including high reactivity, good photostability, non-toxicity and moderate cost (Zhao et al., 2007). The photodecomposition products of MPs vary widely depending on the type of polymer, the type of semiconductor used and the reaction conditions (Tian et al., 2019). Some authors such as Llorente García et al. (2020) or Ariza et al. (2020) claim that photocatalysis of MPs in WWTPs using photocatalysts composed of TiO_2 is feasible. One of the problems that photocatalysis has is the appearance of by-products but in the case of PP, the most abundant by-products formed are acetaldehyde, acetic acid, acetone and formaldehyde. These by-products are considered to be of low toxicity (Uheida et al., 2021).

Therefore, the main objective of this study is to evaluate the degradation of polypropylene particles after the synthesis of three different catalysts, ZnO/TiO_2, CeO_2/TiO_2, and $ZnO\text{-}CeO_2/TiO_2$, under UV-A and UV-B irradiation, as well as to assess the potential toxicity of the resulting degradation products using *Phaeodactylum tricornutum* as a biological model.

2. Materials and methods

2.1. Reagents and materials

Filters (0.8 μm polycarbonate filters PC membrane 47 mm) were supplied by IsoporeTM (Darmstadt, Germany). Hexahydrated cerium nitrate ($Ce(NO_3)_4$–6 H_2O, 99.99 %) and PP ($(C_3H_6)_n$, 99 %) was commercialized by Sigma Aldrich (Madrid, Spain). Iron II sulphate 7-hydrate purissimum, sulphuric acid 95–98 % and hydrogen peroxide 30 % v/v (pure, pharma grade) marketed by Panreac (Barcelona, Spain). Absolute methanol (CH_4O) marketed by Merck (Madrid, Spain). Titanium dioxide (TiO_2, P25) was supplied by Evonik Industries (Essen, Alemania). Zinc nitrate hexahydrate ($Zn(NO_3)_2$–6 H_2O, 98.5 %), Nitric acid (HNO_3, 60 %), Sodium hydroxide and Sodium chloride extra pure were purchased from Scharlab. Acetone (C_3H_6O, Ph. Eur.) was supplied by VWR Chemicals (Barcelona, Spain).

2.2. Chemical experimental procedure

2.2.1. Catalyst synthesis

Three catalysts were synthesized: a) zinc oxide on titanium dioxide (ZnO/TiO_2); b) cerium dioxide on titanium dioxide (CeO/TiO_2); c) zinc oxide doped with cerium dioxide on titanium dioxide ($ZnO\text{-}CeO_2/TiO_2$).

ZnO/TiO_2: ZnO was deposited on TiO_2 by the incipient wetness impregnation method. This catalyst was synthesized with 10 % by weight ZnO and 90 % TiO_2 (Ebrahimbabaie et al., 2022). Photocatalytic decomposition of PE and PS microspheres was performed using TiO_2 nanopellets under UV irradiation. TiO_2 films caused almost complete decomposition (98.4 %) of PS microspheres within 12 h and PE MPs also underwent substantial photodegradation after 36 h (Ariza et al., 2020). Recent studies indicate that the TiO_2–ZnO composite exhibits superior photocatalytic efficiency compared to the individual oxides (Halim et al., 2025). As ZnO precursor, zinc nitrate hexahydrate salt $Zn(NO_3)_2$–6 H_2O was used. A 0.75 M aqueous solution was prepared with this precursor. To carry out the impregnation, the TiO_2 powder was deposited on a ceramic crucible and then the 0.75 M Z $Zn(NO_3)_2$–6 H_2O solution was added drop by drop, at room temperature, over the entire surface of the titanium dioxide. With the help of a rod, the sample was slowly stirred to facilitate the formation of a wet paste, until the final impregnation point was reached. It was then dried in an oven at 105 °C for 24 h. The number of impregnation-drying-milling cycles necessary to obtain a final loading of 10 % by weight in ZnO on TiO_2 was carried out. Specifically, three impregnation cycles were required. Then, after the last grinding, sieving was performed using a sieve with a 75 μm mesh size. Finally, the sample was calcined in air in a muffle furnace at 500 °C for 1 h with a heating ramp of 5 °C/min until reaching 500 °C to decompose zinc nitrate into zinc oxide.

CeO/TiO_2: The incipient wetness impregnation method was also used for the preparation of this catalyst. The present catalyst was synthesized with 30 % by weight of CeO_2 and 70 % by weight of TiO_2 (Shi et al., 2016), 30 % CeO_2 is the most effective percentage by weight over TiO_2 to obtain the highest effectiveness of this catalyst. In this study it is also stated that CeO/TiO_2 mixed oxides have much higher catalytic activities than pure CeO_2 or TiO_2. Another study (Mandal and Pradhan, 2022) uses 20 wt% CeO_2 and 80 wt% TiO_2 for the removal of an organic dye (RhB) in wastewater, achieving a removal of 63 %. Moreover, in this study (Junwei et al., 2022), a high photocatalytic performance of hydrogen evolution and dye degradation was obtained by CeO_2-modified TiO_2 nanotube arrays, where it is exposed that the CeO_2/TiO_2 photocatalyst has excellent potential in dye wastewater purification and new energy development due to the attractive photocatalytic ability. As a precursor of CeO_2 the cerium nitrate hexahydrate salt $Ce(NO_3)_4$–6 H_2O was used. With this precursor a 1M aqueous solution was prepared. All steps were conducted in accordance with the procedures used in the other synthesis.

$ZnO\text{-}CeO_2/TiO_2$: To prepare this catalyst, the incipient wetnes impregnation method was also used. This catalyst was synthesized with the amounts of ZnO and CeO_2 mentioned in the previous catalyst preparations, i.e. 10 % by weight of ZnO, 30 % of CeO_2 and 60 % of TiO_2. $ZnO\text{-}CeO_2/TiO_2$ catalyst was prepared by co-impregnation starting from Ce and Zn precursors as mentioned above. The impregnation-drying-milling cycle was performed three times until a loading of 10 % in ZnO and 30 % in CeO_2 on TiO_2 was obtained.

2.2.2. Physicochemical analysis

The characterization of the synthesized catalysts was carried out by dynamic light scattering (DLS), volumetric nitrogen adsorption-desorption at −196 °C, inductively coupled plasma atomic emission spectroscopy (ICP-AES), X-ray diffraction (XRD), X-ray fluorescence (XRF), electron microscopy, diffuse reflectance spectroscopy.

The hydrodynamic size was measured by using a Malvern Zetasizer Nano-ZS (Malvern Instruments). Textural characterization of the synthesized photocatalysts was performed using the N_2 adsorption-desorption technique at liquid nitrogen temperature (−196 °C). This analysis allows the determination of the adsorption isotherm, following the IUPAC classification (Rouquerol et al., 1999), as well as the specific surface area of the photocatalysts using the BET model (Brunauer, Emmett and Teller) and the total pore volume through the BJH method (Barret, Joyner and Halenda). Volumetric nitrogen adsorption measurements were carried out using a Micromeritics automatic analyzer, model ASAP 2020. Before starting the analysis, the samples were subjected to evacuation under vacuum at 200 °C for 2 h, with the purpose of eliminating adsorbed species on the surface, thus ensuring accuracy in the textural characterization of the material. The composition of the catalysts were measured by inductively coupled plasma atomic emission spectroscopy (ICP-AES) in a spectrometer, model Iris Interpid of Thermo Elemental. In addition, it has also been used to see if there is leaching for catalysts once the catalyst has been separated from the reaction medium. The chemical composition of the catalysts was also analysed by X-ray fluorescence (XRF).

The structural study of the synthesized photocatalysts was carried out using X-Ray Diffraction with a Bruker AXS model D8 Advance powder diffractometer. The radiation used was Cu Kα, operating the X-ray tube at 40 KV and 40 mA; and a scanning range (2θ): 3°–75°. The phase identification study was carried out using PowderCell2.4 software. Electron microscopy was performed using a Thermo ScientificTm Talos F200X scanning/transmission microscope (S/TEM) that combines high-resolution S/TEM and TEM imaging with X-ray scattering spectroscopy signal detection and 3D with compositional mapping. Diffuse reflectance spectroscopy was used to study the Band-gap, which is a technique that allows observing the transition of electrons from the valence band (VB) to the conduction band (CB), in order to calculate the band energy. The technique is carried out with a scanning range of 200–800 nm.

2.2.3. Microparticles characterization

The analysis of PP particles before and after exposure to photocatalysis processes was carried out using a Carl Zeiss Axio Imager M1m optical microscope. Initially, commercial PP particles were sieved to select sizes between 400 and 600 μm, from which those within the range of 500–550 μm were chosen. Particle characterization was performed based on diameter and area measurements. To determine the size distribution in the sample population, a total of 70 particles were analysed, obtaining an average area of 0.190 ± 0.052 μm^2 and its corresponding standard deviation (SD). In each assay, all the particles used were evaluated individually to ensure the accuracy of the results.

2.2.4. FT-IR analysis

After the characterization of the polypropylene (PP) microparticles before and after their exposure to photocatalysis, they were analysed by Fourier transform infrared spectroscopy (FT-IR). For this purpose, a PerkinElmer Spectrum 3 spectrophotometer was used in Attenuated Total Reflectance (ATR) mode. A reference spectrum of the polypropylene was generated, which allowed comparison of the structural modifications in the PP particles after photocatalytic treatment, in relation to the spectrum obtained prior to exposure (Fig. 1). The determination of the initial structure of the particles is crucial to evaluate possible alterations induced by the degradation process.

For the particles studied, bands corresponding to asymmetric (νas) and symmetric (νs) stretching vibrations of the -CH_3 and -CH_2 functional groups were identified in the 2950, 2917, 2868 and 2837 cm-1 regions. Also, asymmetric (δas) and symmetric (δs) deformation bands were observed in the C-H plane at 1457 and 1376 cm-1, along with an additional bending band (δbalance) below 1167 cm-1. Each microparticle was analysed by 4 scans in the spectral range between 4000 and 650 cm-1, with a spectral resolution of 4 cm^{-1}. To ensure the reliability of the data, a background correction was performed every five microparticles analysed, adapted to the specific conditions of the laboratory.

2.2.5. Photocatalytic activity tests on polypropylene microparticles

A total of nine tests were performed to study the degradation. 6 tests for the catalysts (ZnO/TiO_2, CeO/TiO_2 and ZnO- CeO_2/TiO_2) considering the two types of light (UV-A and UV-B). In addition, 2 more tests were performed, one for each type of light to test the possible degradation of UV-A or UV-B light in aqueous medium without the effect of the synthesized catalyst. All samples were run in duplicate. Finally, the most efficient catalyst was tested with urban wastewater and PP particles under study.

An initial control of the luminous intensity emitted by the lamps used was carried out to ensure the accuracy of the irradiation process. A UVP radiometer with an associated sensor was used for this purpose, which allows a direct and precise measurement of the radiation. The sensor facilitates the approach to the emission source, registering an intensity of 20 mW/cm^2, guaranteeing optimal conditions for the development of the experiment.

For determining the influence of photocatalysis on the degradation

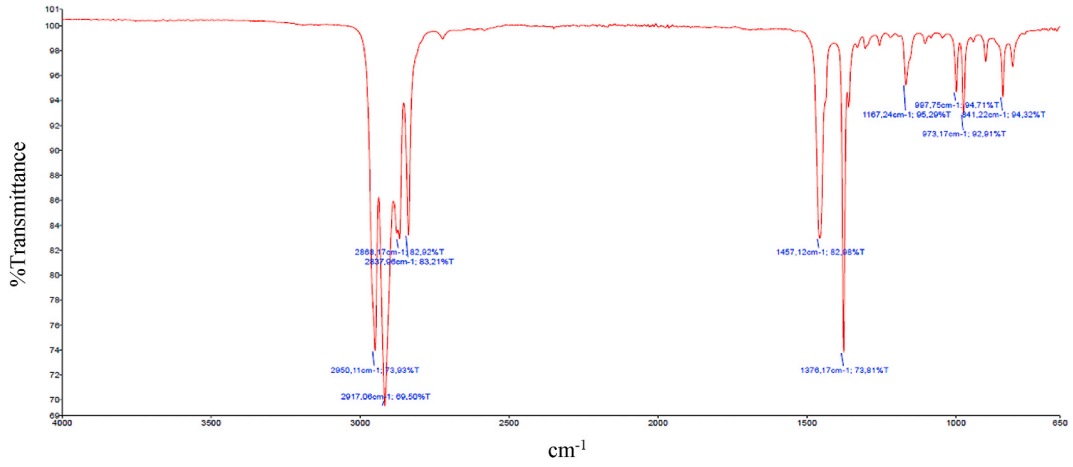

Fig. 1. Reference PP microparticle FTIR-ATR spectrum.

of polypropylene (PP) particles, a concentration was established based on previous studies of Medina Sidonia wastewater treatment plant (WWTPs), according to data reported by Martín-García et al. (2023). Microplastic concentrations ranging from 10.6 MP/L to 793.5 MP/L were identified in these systems. According to the above results, 10 previously characterized PP particles were selected and suspended in 100 mL of ultrapure water with a loading of 2.5 g/L of catalyst. These samples were subjected to constant agitation at 200 rpm for 48 h, while UV-A or UV-B irradiation was applied to evaluate the effects of the photocatalytic process on the degradation of the polymeric material. This procedure allowed observing possible structural modifications derived from the interaction between the catalyst and the PP particles in a controlled environment.

2.3. Quality assurance and quality control

Properties of the selected polymer, including its shape and size, minimize the risk of cross-contamination. However, to ensure an interference-free environment throughout the experimental process, stringent control measures were implemented. All equipment used was previously washed in multiple cycles with distilled water and protected with aluminum foil, avoiding any possible introduction of external particles. During the sampling and analysis stages, cotton gowns and gloves were used in order to reduce contamination by synthetic fibers. Additionally, all reagents were pre-filtered using a 0.45 μm glass fiber filter.

2.4. Test organism

2.4.1. Sample preparation and standardization

To ensure comparability among treatments and avoid confounding effects due to differences in salinity, all environmental samples were first adjusted to a standard salinity of 36, equivalent to that of natural seawater. Initial salinity values of the raw samples were measured using a calibrated salinometer, yielding the following values (in PSU): Water only with UV = 73, Water with PP-MPs + UV = 112, Water with PP-MPs + UV + ZnOTiO2 = 112–156 and MPs + UV + ZnOCeO2/TiO2 = 80-86.

To adjust the salinity, 5 mL of each sample were prepared by diluting appropriate volumes of the original samples with ultrapure water.

Following salinity adjustment, pH values were fine-tuned by stepwise addition of either 1.01 % (w/v) NaOH or 0.35 % HCl, in increments no greater than 2 μL, to minimize overshooting. The final pH of all samples was standardized to 8.2 ± 0.05, a range considered non-inhibitory to microalgal growth.

2.4.2. Marine microalgae ecotoxicity test

The marine microalgae assays were performance following the OECD guidelines N° 201; Algal Growth Inhibition Test. The marine diatom *Phaeodactylum tricornutum* BACILLARIOPHYCEAE (Bohlin, 1897), strain CCMM 07/0402, obtained from the ICMAN Marine Microalgae Culture Collection (CCMM), was selected as the test organism. The microalgae selected was chosen because it is a standard species used in toxicology tests (ISO, 1995).

The assay was conducted in white, flat-bottom 96-well microplates suitable for fluorescence measurements. Each well had a final volume of 300 μL, composed of 200 μL of test sample (undiluted or serially diluted to 50 %, 25 %, or 12.5 % with sterile 0.2 μm-filtered natural seawater) and 100 μL of algal suspension.

The algal suspension contained 3×10^4 cells·mL^{-1}, resulting in a final initial concentration of 1×10^4 cells·mL^{-1} in each well. The suspension also included f/2 medium (without EDTA and trace metals; Guillard and Ryther, 1962) and a silicate solution at 150 mg L^{-1}, which diluted to the standard f/2 concentration upon mixing with the sample, in order to reach 50 mg L^{-1} of silicate in the well. All treatments and dilutions were performed in triplicate. Twelve control wells (filtered seawater + algal suspension) were included per plate. Peripheral wells (first and last columns and rows) were excluded from analysis and filled with 300 μL of filtered seawater to minimize edge evaporation effects, allowing for 60 effective test wells per plate.

Plates were incubated at 20 °C under continuous light. Homogeneous light exposure was ensured by placing the plates on a rotating platform. Chlorophyll fluorescence was monitored daily as a proxy for algal growth. On the final day (72 h post-exposure), cell density may be quantified via flow cytometry if needed to corroborate fluorescence-based results. Baseline measurements taken at time zero confirmed uniform algal distribution across all wells, validating the seeding process.

2.4.3. Flow cytometry analysis

Flow cytometric analyses were carried out at 24, 48, and 72 h using an Accuri C6 flow cytometer equipped with a 488 nm excitation laser. Cell populations were characterized based on forward scatter (FSC), side scatter (SSC), and fluorescence collected with a 670 nm long-pass filter (FL3), which correspond to cell size, internal complexity, and the autofluorescence of chlorophyll *a* (ChlA), respectively (Shapiro, 2003). These parameters were measured across all concentrations tested, allowing for the assessment of microalgal growth.

2.4.4. Statistical analysis

All bioassays were carried out in triplicate. Data are shown as average ± standard deviation between replicates. The growth inhibition values were fitted to the Hampel model (Hampel et al., 2001), with different concentrations tested, in order to calculate the effective values for 50 % inhibition after 72 h (EC50) of microalgae cellular concentration.

3. Results and discussion

3.1. Catalysts characterization

3.1.1. Compositional characterization by XRF and ICP-AES

Analysis of the composition of the photocatalysts was carried out using X-ray fluorescence (XRF) and inductively coupled plasma optical emission spectroscopy (ICP-AES), obtaining results expressed in mass percentage ([wt]%). These techniques allowed us to evaluate the presence and distribution of elements in the materials, providing key information to determine their photoactive behaviour. The comparison between the experimental results and the nominal composition of the photocatalyst allowed validating the synthesis and confirming the proper integration of the semiconductor in the catalytic matrix. Table 1 shows the measured weight percentage of the different elements found in each catalyst and, in parentheses, the nominal percentage. All catalysts exhibit elemental compositions that are consistent with their nominal values.

3.1.2. Structural study

X-ray diffraction allows to study the crystal structure of the synthesized photocatalysts (Fig. 2)

The diffractogram (Fig. 2) shows the peaks of hexagonal ZnO, fluorite-type CeO_2 and rutile (rutile) TiO_2 structures. Most of the

Table 1
Compositional characterization by XRF for ZnO/TiO_2, CeO_2/TiO_2 and ZnO-CeO_2/TiO_2 photocatalysts.

Composition (%weight)			
Catalysts	**Zn**[a]	**Ti**[b]	**Ce**[b]
ZnO/TiO_2	8.8 (10)	87.2 (90)	–
CeO_2/TiO_2	–	73.1 (70)	26.8 (30)
ZnO-CeO_2/TiO_2	10.1 (10)	58.7 (60)	25.4 (30)

[a] Measured by ICP.
[b] Measured by XRF.

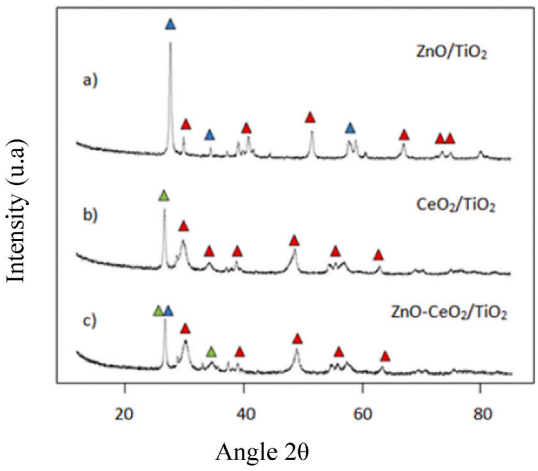

Fig. 2. Diffractogram of the ZnO/TiO_2 (a), CeO_2/TiO_2 (b) and $ZnO\text{-}CeO_2/TiO_2$ (c) catalysts by XRD technique. The blue color represents the peaks corresponding to the hexagonal ZnO phase, the red color the peaks of the TiO_2 (rutile) phase and the green color the peaks of the fluorite-type CeO_2 phase.

diffraction peaks are associated with the rutile TiO_2 phase (JCPDS 021–1276). However, for the hexagonal ZnO hexagonal phase (JCPDS 036–14519) only 3 diffraction peaks can be assigned, which are (110), (004) and (310). The diffraction peak that stands out the most is the one corresponding to the (110) plane which can also be observed in the $ZnO\text{-}CeO_2/TiO_2$ catalyst. For the fluorite-type CeO_2 phase (JCPDS 034–0394**)**, the most intense peak that we observed in the CeO_2/TiO_2 catalyst correspond to the (111) plane, which coincides in the (110) plane of the hexagonal ZnO in the $ZnO\text{-}CeO_2/TiO_2$ catalyst. Other possible phases such as TiO_2 anatase cannot be disregarded. Although they do not appear clearly in the diagrams because they form very low intensity peaks and are confused with the base, it is possible that they are found forming mixtures or smaller crystals. For this purpose, a refinement has been carried out using the Powder Cell program. The volume percentage obtained for each phase is shown in Table 2.

Considering Tables 2, it can be stated that the catalysts are mostly constituted by TiO_2 (rutile). It has also been studied whether the catalysts were composed of TiO_2 (anatase) but it was observed that this TiO_2 phase was not found in any catalyst. The lattice parameters of each of the phase's present in the catalysts have been obtained and are shown in Table 3.

In all cases, the lattice parameters obtained after refinement are similar to those of the corresponding theoretical structures (JCPDS cards), with the exception of the rutile phase observed in the CeO_2/TiO_2 and ZnO/TiO_2 catalysts. In the CeO_2/TiO_2 catalyst, the lattice parameter of TiO_2 increases, whereas in the ZnO/TiO_2 catalyst, a decrease in the lattice parameter is observed. These variations are consistent with literature (Haffad and Korir, 2019) and are attributed to lattice distortion in the rutile structure, caused by the interaction of the CeO_2 fluorite phase and ZnO hexagonal phase with the rutile TiO_2. In the case of the $ZnO\text{-}CeO_2/TiO_2$ catalyst, this effect is likely not observed due to the opposing influences: the lattice expansion induced by CeO_2 and the contraction caused by ZnO effectively compensate each other.

Table 2
Volume percentages obtained of each phase of the compounds that form the catalysts by XRD obtained through Powder Cell.

Catalysts	TiO_2 tetragonal rutile (%)	ZnO hexagonal (%)	CeO_2 fluorite type (%)
ZnO/TiO_2	63.6	36.4	–
CeO_2/TiO_2	87.8	–	12.2
$ZnO\text{-}CeO_2/TiO_2$	57.4	36.8	5.8

3.1.3. Electron microscopy (HAADF-XEDS)

By means of electron microscopy it is possible to know at the nanometer scale whether the catalysts are homogeneous. Specifically, HAADF-XEDS was used to take the different images of the catalysts (Fig. S1).

Figures S1a, S1b and S1c show different colours according to the distribution of Ti (red), Zn (green) and Ce (blue) in the 3 catalysts. It is observed that the 3 elements are homogeneously distributed in the catalyst. TiO_2 is the main component of these catalysts as prepared. Table 4 shows the composition of the catalysts at the nanometer scale. Owing to the homogeneous distribution of Zn and Ce on the TiO_2 surface, the compositional analysis of selected surface regions matches the nominal values.

3.2. Textural properties

Textural characterization of the synthesized photocatalysts was carried out by performing volumetric adsorption-desorption isotherms of N_2 at 77K, and the application of the BET method (Brunauer, Emmett and Teller) for the determination of the specific surface area of each of the catalysts. In addition, the BJH method (Barret, Joyner and Halenda) has been applied to obtain the pore volume of the catalysts surface. The adsorption/desorption isotherm of catalysts is represented in Fig. S2. According to the isotherm classification recommended by IUPAC (Rouquerol et al., 1999), all catalysts correspond to a type IV isotherm.

In addition, the values corresponding to the specific surface area and pore volume of the catalysts analysed are detailed in Table 5, providing key data to evaluate their efficiency in catalytic processes. The CeO_2/TiO_2 catalyst exhibits the highest specific surface area, followed by ZnO/TiO_2. In contrast, the catalyst prepared via co-impregnation shows the lowest specific surface area among the samples analysed.

3.2.1. Band-Gap

Band-Gap of the photocatalysts has been obtained using UV–Vis absorption data. In this way, diffuse reflectance data is obtained. Fig. 3 gives a strong absorption that increases as the wavelength decreases. The absorption occurs at a certain wavelength, the value of which we can obtain from the graph to determine the band gap energy. The band gap energy is calculated using eq. (1):

$$E = \frac{1240}{\lambda\,(nm)} eV \qquad \text{(eq.1)}$$

The catalyst with the highest catalytic activity is the one with the lowest band gap. The wavelength values were 390, 440 and 320 nm for ZnO/TiO_2, CeO_2/TiO_2 and $ZnO\text{-}CeO_2/TiO_2$, respectively. The energy obtained was 3.18, 2.82 and 3.88 eV for ZnO/TiO_2, CeO_2/TiO_2 and $ZnO\text{-}CeO_2/TiO_2$, respectively. Therefore, once the band gap for each catalyst has been calculated, we can conclude that the catalyst composed of CeO_2/TiO_2 has the smallest band gap. A small band gap in semiconductor materials has several advantages, as they require less energy for the transfer of electrons from the valence band to the conduction band; this results in higher electron mobility and therefore better conductivity, as well as allowing more efficient use of light radiation (Saquib et al., 2024).

3.2.2. Dynamic light scattering (DLS)

DLS technique was used to know the size of the catalyst aggregates in solution. Since this reaction occurs in the aqueous phase, determining the size of the suspended particles is crucial. In Fig. S3, it is shown that the size of the different catalysts is less than 100 nm. For all three catalysts, the hydrodynamic particle size is comparable, ranging from approximately 100 to 6000 nm, with the majority of the population concentrated between 1000 and 2000 nm.

Table 3
Lattice parameters of each of the phase's present in the catalysts through XRD. The lattice parameters from the JCPDS files for rutile TiO_2, hexagonal ZnO, and fluorite CeO_2 are shown in brackets.

Catalysts	TiO_2 tetragonal rutile		ZnO hexagonal		CeO_2 fluorite type
	a (Å)	b (Å)	a (Å)	b (Å)	a (Å)
ZnO/TiO_2	4.594 (4.93)	2.959 (2.959)	3.257 (3.25)	5.207 (5.2)	–
CeO_2/TiO_2	5.207 (4.593)	2.964 (2.959)	–	–	5.409 (5.411)
$ZnO\text{-}CeO_2/TiO_2$	4.594 (4.593)	2.958 (2.959)	3.255 (3.25)	5.230 (5.2)	5.410 (5.411)

Table 4
Mass weight percentages of Ti, Zn and Ce in the different catalysts by electron microscopy.

Catalysts	Chemical element	Composition (% weight)	Nominal composition (% weight)
ZnO/TiO_2	**Ti**	88.3	90
	Zn	11.7	10
CeO_2/TiO_2	**Ce**	34.9	30
	Ti	65.1	70
$ZnO\text{-}CeO_2/TiO_2$	**Zn**	10.0	10
	Ti	58.2	60
	Ce	31.8	30

Table 5
Results of surface area, volume and pore size when performing the N_2 adsorption-desorption technique on the catalysts studied.

	Surface BET (m^2/g)	Pore volumen BJM (cm^3/g)	Pore size (Å)
ZnO/TiO_2	40.5	0.3	282.7
CeO_2/TiO_2	49.7	0.2	165.3
$ZnO\text{-}CeO_2/TiO_2$	33.1	0.2	183.8

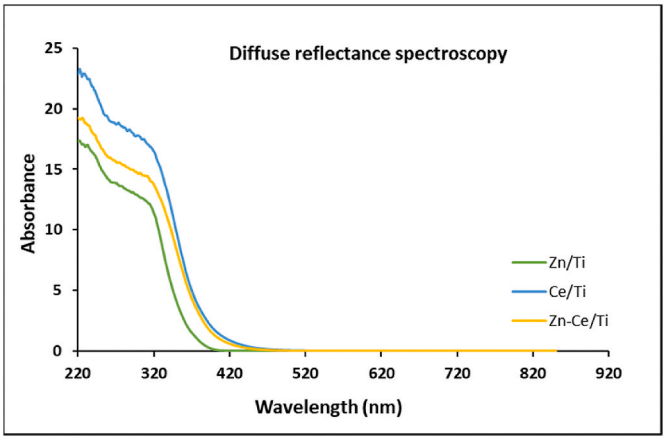

Fig. 3. Diffuse reflectance spectroscopy applied to the catalysts studied (ZnO/TiO_2, CeO_2/TiO_2 and $ZnO\text{-}CeO_2/TiO_2$).

3.3. Photocatalytic activity for degradation of polypropylene microplastics

In order to evaluate the effect of UV radiation on the degradation of microplastics without the intervention of a photocatalyst, a study was carried out on 10 polypropylene (PP) particles, evaluating changes in their surface area before and after exposure. The comparison between the initial and final average area made it possible to quantify the effect of the different radiations applied in the absence of the catalyst. This analysis provides an estimate of the percentage of degradation, showing how UV radiation acts directly on the particles without additional catalytic processes. The observed degradation is attributed exclusively to the interaction of the different wavelengths of radiation with the polymeric material, providing a baseline reference for comparative studies with synthetic photocatalysts.

Photocatalyst with the highest performance was the one formed by ZnO/TiO_2 and UV-A with which a degradation percentage of 8.4 % of the PP particles was obtained (Table 6). Ge et al. (2022) investigated the high photocatalytic activity of ZnO and TiO_2 for the degradation of MPs under UV light, in particular, the photocatalytic degradation of a PVC–ZnO composite film in the presence of a sensitizing dye (eosin Y) under UV irradiation resulted in a 20 % mass loss after 4 h. In this other study (Yusuff et al., 2022), ZnO/TiO_2 photocatalyst was used under sunlight for the removal of methylene blue dye, in which almost complete decolorization of dye molecules in wastewater was achieved within 60 min. This photocatalyst showed great potential as a low-cost, visible light-sensitive photocatalyst for degradation/decolorization of dye-containing wastewater.

CeO_2/TiO_2 and $ZnO\text{-}CeO_2/TiO_2$ catalysts were not as effective as the one mentioned above, but the degradation of the PP particles was also achieved with these photocatalysts, as can be seen in Table 6. In the blank performed in tests 3 and 4 it can be observed that the UV-A lamp degrades 2.5 % and the UV-B lamp 3.1 % to the MPs.

Test 10 was conducted using 100 mL of water from the Medina WWTP and the ZnO/TiO_2 catalyst, which resulted in the highest degradation percentage. A degradation of 6.6 ± 1.6 was obtained, which is below 8.4 ± 1.0 with pure water, due to interactions of organic matter and other compounds present in the WWTP outlet water.

Fig. 3 shows the characteristic bands and peaks of the untreated PP. At 1457 cm^{-1} is the part of the asymmetric bending of CH_3; this band coincides with the bending of CH_2. The symmetric bending appears at 1375 cm^{-1}. The bands between 1164 cm^{-1} and 812 cm^{-1} correspond to the vibration of the CH_3 skeleton. It is observed that towards 3000-2800 cm^{-1} the CH stresses appear. The peak at about 1040 cm^{-1} is assigned to the vibrational stretching of the hydrogen- or alcohol-bonded hydroxyl groups (-O-H) and superoxide groups (-O-O-H). We can assign vibrational and asymmetric bending for the C-H bonds between the peaks found between 1490 and 900 cm^{-1} (Zhang et al., 2018).

The changes on the PP surface caused by photocatalytic deterioration were determined by ATR-FTIR spectroscopy (Fig. 4). This equipment can determine the alterations of functional groups on the surface of PP particles down to several microns. A rather limited degradation is observed since the photocatalyst has degraded 9.4 % of the PP particle. Darvish et al. (2020) show that 1500 mg of PP were reacted with 100 mg of carbonized TiO_2 in 100 mL of distilled water under UV-C light for 400 h, obtaining a degradation of 84.3 %. In this other study (Pino et al.,

Table 6
Degradation of PP microplastics, expressed in area variation (in %) after photocatalytic experiments.

	Degradation (%)	
Catalysts	UV-A	UV-B
—	2.5 ± 0.4	3.1 ± 1.1
ZnO/TiO_2	8.4 ± 1.0	8.2 ± 0.4
CeO_2/TiO_2	5.2 ± 2.2	3.4 ± 0.6
$ZnO\text{-}CeO_2/TiO_2$	6.1 ± 2.0	3.4 ± 1.2

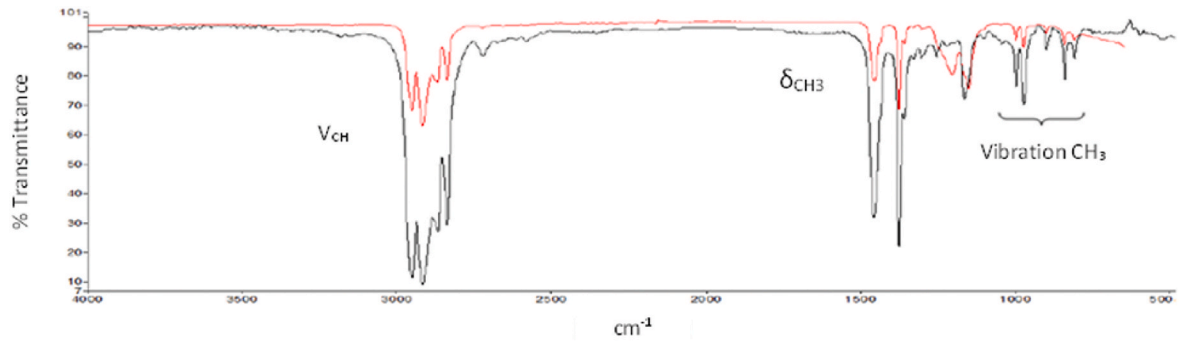

Fig. 4. Comparison of reference PP spectrum (▬) compared to PP subjected to ZnO/TiO_2 (▬).

2021), more than 65 % of the MPs were degraded by reacting them with ZnO nanowires under visible light irradiation for 2 weeks.

Saifuddin et al. (2022) affirm that LDPE films were placed on the surface of a TiO_2 powder layer and then exposed to UV radiation for 3, 5, 7 and 9 days. Similar ATR-FTIR spectra were obtained for both the molecular structure of the LDPE film and the existence of a carbonyl-based functional group. However, compared to the results obtained by using UV radiation alone, it could be observed that the use of TiO_2 together with UV radiation was able to enhance the degradation rate of the LDPE film. This is due to the generation of highly oxidizing radicals on the TiO_2 surface through the photoinduced redox reaction, which could damage the molecular structure of the LDPE film.

3.4. Catalyst leaching studies

Once the catalysts were separated from the reaction medium, the possible leaching of the catalyst in the reaction medium was analysed using the ICP technique. The separation of the reaction medium was carried out by centrifugation, which was carried out for 10 min at 5000 rpm. Table 7 shows that the concentration of Ce is low, so there is no leaching of cerium. However, as for Ti, there is an appreciable concentration in the catalysts formed by ZnO/TiO_2 and ZnO-CeO_2/TiO_2. Finally, as for Ti, there is no leaching in any of the catalysts since it is found in very low concentrations.

Leaching of elements that are part of the catalysts into the reaction medium is important as it can become a source of secondary contamination of the aqueous medium in which it is applied (Inturi et al., 2016). In addition, leaching of these elements can lead to a gradual loss of catalytic efficiency (Gruber-Woelfler et al., 2012). Some authors have addressed the influence of the method of synthesis of the catalyst on its predisposition to subsequent leaching (Inturi et al., 2016). This is an aspect that should not be ignored, and, in this study, the concentrations of Ti found in the water after the photocatalytic experiment suggest that leaching should be an aspect to be studied further.

3.5. Microalgae toxicity test

Treatments with PP-MPs resulted in significant growth inhibition of *Phaeodactylum tricornutum* compared to the control containing only UV-exposed water. Significant differences in toxicity were observed between the two tested photocatalysts (Fig. 5). The ZnO-CeO_2/TiO_2 catalyst caused lower growth inhibition, whereas no significant differences were observed between the PP-MPs + UV control and the treatment with the ZnO/TiO_2 catalyst. Nonetheless, significant differences were detected between the two catalysts.

These results suggest that the presence of photocatalysts influences the toxicity of UV-aged PP-MPs toward *Phaeodactylum tricornutum*. The reduced growth inhibition observed with the ZnO-CeO_2/TiO_2 catalyst indicates a potentially lower generation of toxic by-products or more effective degradation of harmful compounds. In contrast, the similar toxicity levels between the ZnO/TiO_2 treatment and the PP-MPs + UV control suggest that this catalyst could not mitigate the adverse effects of UV-aged microplastics. The significant differences observed between the two catalysts highlight the importance of catalyst composition in determining the environmental safety of photocatalytic treatments.

Table 7
Ce, Zn and Ti concentrations applied by ICP technique.

Concentration (mg/L)			
Catalysts	Zn	Ti	Ce
ZnO/TiO_2	–	17.0 ± 0.1	0.022 ± 0.003
CeO_2/TiO_2	<0.100	–	<0.005
ZnO-CeO_2/TiO_2	<0.100	16.0 ± 0.1	0.020 ± 0.004

4. Conclusions

Synthesis technique revealed promise for the fabrication of these 3 TiO_2-based catalysts. ZnO, CeO_2 and TiO_2 catalysts have been tested in combination with two types of ultraviolet light (UV-A and UV-B) for the removal of polypropylene (ranging from 500 to 550 μm) in pure and wastewater matrices. A higher percentage of degradation was obtained for ZnO/TiO_2. The results obtained were 8.4 ± 1.0 (UV-A) and 8.2 ± 0.4 (UV-B). For wastewater a degradation of 6.6 ± 1.6 was obtained. In addition, another factor to consider is that the study of the leaching of the catalysts showed that a minimum part of the catalyst formed by ZnO/TiO_2 remains in the aqueous solution. The ZnO-CeO_2/TiO_2 catalyst resulted in lower growth inhibition compared to ZnO/TiO_2, which showed toxicity levels similar to those of UV-aged PP-MPs without catalyst, highlighting the role of catalyst composition in modulating the environmental toxicity of degraded microplastics. A limitation identified was the inefficient recovery of the catalyst, which highlights the need for future research aimed at developing novel supports capable of maintaining or even enhancing catalytic performance. These efforts should focus on designing systems that enable easier and less costly recovery and reuse of the catalyst, thereby improving the overall sustainability and feasibility of the process.

CRediT authorship contribution statement

A. Egea-Corbacho: Writing – original draft, Methodology, Investigation, Formal analysis, Conceptualization. **A.P. Martín-García:** Writing – original draft, Methodology, Conceptualization. **J.M. Salas-Calvo:** Investigation, Formal analysis, Data curation. **D. Coello:** Supervision, Resources, Methodology. **R. Rodríguez:** Writing – review & editing, Resources, Project administration, Funding acquisition, Formal analysis. **I. Moreno-Garrido:** Supervision, Methodology, Conceptualization. **M. Sendra:** Writing – original draft, Methodology, Investigation, Data curation. **M.P. Yeste:** Writing – review & editing, Supervision, Project administration, Funding acquisition, Formal analysis.

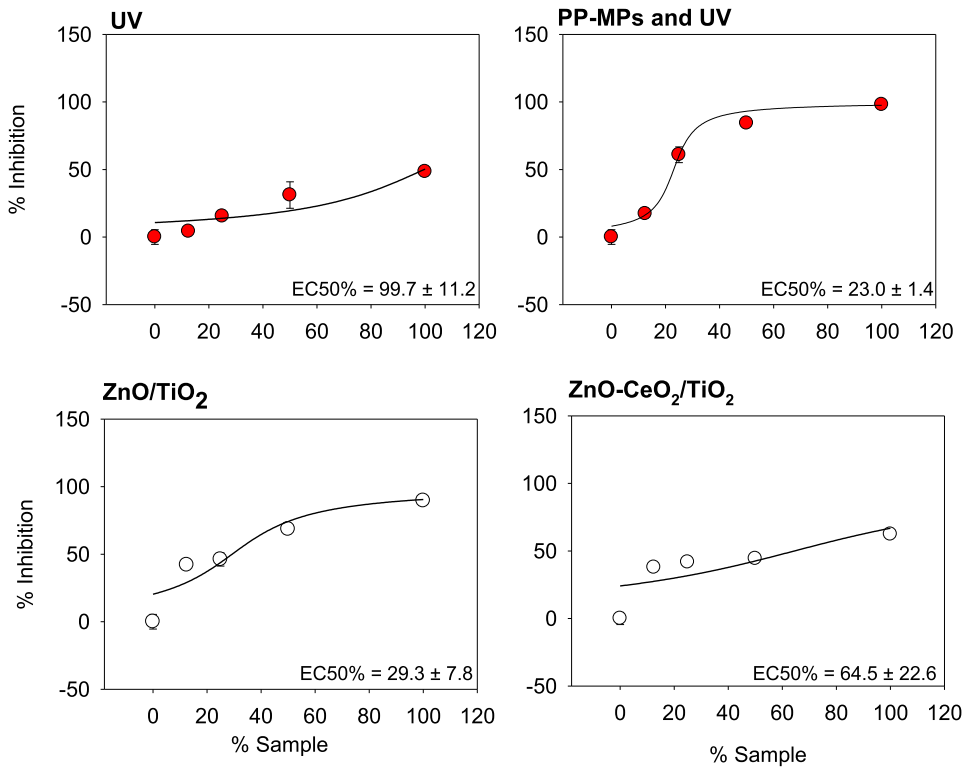

Fig. 5. Percentage of growth inhibition of *Phaeodactylum tricornutum* exposed to different proportion of tested water which it was in contact i) only with UV, ii) PP-MPs + UV and iii) both catalysts which showed metal leachates with the PP-MPs + UV. EC50 % is shown in each sigmoidal curve analysed.

Declaration of competing interest

The authors declare that they have no known competing financial interests or personal relationships that could have appeared to influence the work reported in this paper.

Acknowledgements

This work was supported by Spanish Ministry of Science and Innovation, specifically via the project PID2022-141731OB-I00, entitled "Potabilization technologies for the elimination of emerging contaminants in the presence of microplastics in drinking water, testing of toxic effects", funded by MICIU/AEI/10.13039/501100011033 and by ERDF/EU and the project PID2020–113006-RB-I00.

Appendix A. Supplementary data

Supplementary data to this article can be found online at https://doi.org/10.1016/j.jenvman.2025.127289.

Data availability

Data will be made available on request.

References

Ariza, M., V, J., Barbieri, V., Siligardi, C., Cedillo, E., 2020. New strategy for microplastic degradation: green photocatalysis using a protein-based porous N-TiO2 semiconductor. Ceram. Int. 45 (7), 9618–9624.

Bayo, J., Olmos, S., López, J., 2020. Microplastics in an urban wastewater treatment plant: the influence of physicochemical parameters and environmental factors. Chemosphere 238, 124593. https://doi.org/10.1016/j.chemosphere.2019.124593.

Bohlin, K.H., 1897. Zur Morphologie und Biologie einzelliger Algen. Öfversigt af Kongl. Vetenskaps-akademiens forhandlingar 54 (9), 507 - 529.

Da Costa, J., Nunes, A., Santos, P., Girao, A., Duarte, A., Rocha-Santos, T., 2018. Degradation of polyethylene microplastics in seawater: insights into the environmental degradation of polymers. J. Environ. Sci. Health Part A 53 (9), 866–875. https://doi.org/10.1080/10934529.2018.1455381.

Darvish, F., Mostofi S, N., Khani, M., Eslami, E., Shokri, B. y Mohseni M., 2020. Direct plasma treatment approach based on non-thermal gliding arc for surface modification of biaxially-oriented polypropylene with post-exposure hydrophilicity improvement and minus aging effects. Appl. Surf. Sci. 509, 144815. https://doi.org/10.1016/j.apsusc.2019.144815.

Ebrahimbabaie, P., Yousefi, K. y, Pichtel, J., 2022. Photocatalytic and biological technologies for elimination of microplastics in water: current status. Sci. Total Environ. 806 (Part 2), 150603. ISSN 0048-9697.

Ge, J., Zhang, Z., Ouyang, Z., Shang, M. y, Liu, P., 2022. Photocatalytic degradation of (micro)plastics using TiO2-based and other catalysts: properties, influencing factor, and mechanism. Environ. Res. 209. https://doi.org/10.1016/j.envres.2022.112729.

Gruber-Woelfler, H., Radaschitz, P.F., Feenstra, P.W., Haas, W., Khinast, J.G., 2012. Synthesis, catalytic activity and leaching studies of a heterogeneous Pd-catalyst including an immobilized bis(oxazoline) ligand. J. Catal. 286, 30–40. https://doi.org/10.1016/j.jcat.2011.10.013.

Guillard, R.R.L., Ryther, J.H., 1962. Studies of marine planktonic diatoms: I. Cyclotella nana Hustedt, and Detonula confervacea (Cleve) Gran. Can. J. Microbiol. 8 (2), 229–239. https://doi.org/10.1139/m62-029.

Haffad, S., Korir, K., 2019. Interfacial structure and electronic properties of TiO2/ZnO/TiO2 for photocatalytic and photovoltaic applications: a theoretical study. Surf. Sci. 686, 10–16.

Halim, O.M.A., Mustapha, N.H., Fudzi, S.N.M., Azhar, R., Zanal, N.I.N., Nazua, N.F., Nordin, H.A., Azami, M.S.M., Ishak, M.A.M., Ismail, W.I.I.N., Ahmad, Z., 2025. A review on modified ZnO for the effective degradation of methylene blue and rhodamine B. Results Surf. Interfaces 18, 100408. https://doi.org/10.1016/j.rsurfi.2024.100408.

Hampel, M., Moreno-Garrido, I., Sobrino, C., Lubián, L.M., Blasco, J., 2001. Acute toxicity of LAS homologues in marine microalgae: esterase activity and inhibition growth as endpoints of toxicity. Ecotoxicol. Environ. Saf. 48 (3), 287–292. https://doi.org/10.1006/eesa.2000.2028.

Inturi, S.N.R., Suidan, M., Smirniotis, P.G., 2016. Influence of synthesis method on leaching of the Cr-TiO_2 catalyst for visible light liquid phase photocatalysis and their stability. Appl. Catal. B Environ. 180, 351–361. https://doi.org/10.1016/j.apcatb.2015.05.046.

ISO, 1995. Water quality—Marine Algal growth-inhibition Test with *Skeletonema costatum* and *Phaeodactylum tricornutum* (ISO 10253: 1995). European Committee for Standardization.

Jinhui, S., Sudong, X., Yan, N., Xia, P., Jiahao, Q., Yongjian, X., 2019. Effects of microplastics and attached heavy metals on growth, immunity, and heavy metal accumulation in the yellow seahorse, Hippocampus kuda Bleeker. Mar. Pollut. Bull. 149, 110510. https://doi.org/10.1016/j.marpolbul.2019.110510.

Jovanović, B., 2017. Ingestion of microplastics by fish and its potential consequences from a physical perspective: potential consequences of fish ingestion of microplastic.

Integration Environment Assess Manager 13 (3), 510–515. https://doi.org/10.1002/ieam.1913.
Junwei, H., Yang, H., He, B., Ma, J., Lu, Yuan, y Wang, Q., 2022. High photocatalytic performance of hydrogen evolution and dye degradation enabled by CeO2 modified TiO2 nanotube arrays, 310.
Llorente, B., Hernández, J., Zaldívar, A., Siligardi, C., 2020. First insights into photocatalytic degradation of HDPE and LDPE microplastics by a mesoporous N-TiO2 coating: effect of size and shape of microplastics. Coatings 10 (7), 658.
Mandal, R. y, Pradhan, S., 2022. Enhanced photocatalytic performance of cauliflower-like CeO2-TiO2 nanocomposite for the RhB dye degradation under visible light. Mater. Today 66 (Part 7).
Martín-García, A.P., Egea-Corbacho, A., Franco, A.A., Rodríguez-Barroso, R., Coello, M. D., Quiroga, J.M., 2023. Grab and composite samples: variations in the analysis of microplastics in a real wastewater treatment plant in the south of Spain. J. Environ. Chem. Eng. 11 (2), 109486. https://doi.org/10.1016/j.jece.2023.109486.
Pino, V., Bucio, E. y, Díaz, D., 2021. Fast photocatalytic polypropylene degradation by nanostructured bismuth catalysts. Polym. Degrad. Stabil. 190, 109648. https://doi.org/10.1016/j.polymdegradstab.2021.109648.
Reddy, A., Moniruzzaman, M., Aminabhavi, T.M., 2018. Polychlorinated biphenyls (PCBs) in the environment: recent updates on sampling, pretreatment, cleanup technologies and their analysis. Chem. Eng. J. 358, 1186–1207. https://doi.org/10.1016/j.cej.2018.09.205.
Rouquerol, F., Rouquerol, J., Sing, K., 1999. Introduction. Adsorption by Powders and Porous Solids, pp. 1–26.
Saifuddin, M., Ghaffari, Y., Park, S.Y., Kim, C.G., 2022. Rapid surface degradation of co-axially arranged polypropylene globules by nanoporous carbonized TiO2 assisted with UV-C. Environ. Res. 212, 113422. https://doi.org/10.1016/j.envres.2022.113422.
Saquib, M., Rani, M., Mubashir, T., Tahir, M.H., Maryam, M., Mushtaq, A., Razzaq, R., El-Sheikh, M.A., Elansary, H.O., 2024. Designing of low bad gap organic semiconductors through data mining from multiple databases and machine learning assisted property prediction. Opt. Mater. 150, 115295. https://doi.org/10.1016/j.optmat.2024.115295.
Shapiro, H.M., 2003. Practical Flow Cytometry, fourth ed. Wiley.
Shi, Z., Yang, P., Tao, F. y, Zhou, R., 2016. New insight into the structure of CeO2–TiO2 mixed oxides and their excellent catalytic performances for 1,2-dichloroethane oxidation. Chem. Eng. J. 295, 99–108. https://doi.org/10.1016/j.cej.2016.03.032.
Selvam, S., Jesuraja, K., Venkatramanan, S., Priyadarsi, R.J.V., 2021. Hazardous microplastic characteristics and its role as a vector of heavy metal in groundwater and surface water of coastal South India. J. Hazard Mater. 402, 123786. ISSN 0304-3894.
Schymansk, D., Goldbeck, I., Humpf, H., Fürst, P., 2018. Analysis of microplastics in water by micro-raman spectroscopy: release of plastic particles from different packaging into mineral water. Water Res. 129, 154–162. https://doi.org/10.1016/j.watres.2017.11.011.
Tian, L., Chen, Q., Jiang, W., Wang, L., Xie, H., Kalogerakis, N., 2019. A carbon-14 radiotracer-based study on the phototransformation of polystyrene nanoplastics in water versus in air. Environment Science Nanothecnology 6 (9), 2907–2917.
Uddin, S., Fowler, S., Behbehani, M., 2020. An assessment of microplastic inputs into the aquatic environment from wastewater streams. Mar. Pollut. Bull. 160, 111538. ISSN 0025-326X.
Uheida, A., Mejía, H., Abdel, M., Hamd, W., Dutta, J., 2021. Visible light photocatalytic degradation of polypropylene microplastics in a continuous water flow system. J. Hazard. Mater. 406, 124299.
Wagner, M., Lambert, S., 2018. Freshwater Microplastics. Springer International Publishing. https://doi.org/10.1007/978-3-319-61615-5.
Yusuff, D., Kudirat, A., Adeniyi, O. y Olutoye M., 2022. Siliceous termite hill supported ZnO-TiO2 as a solar light responsive photocatalyst: synthesis, characterization and performance in degradation of methylene blue dye. Surf. Interfaces 34. https://doi.org/10.1016/j.surfin.2022.102360.
Zhang, R. y, Ulery, B.D., 2018. Synthetic Vaccine Characterization and Design, vol. 12. American Scientific Publishers, pp. 1–11.
Zhao, X., Li, Z., Chen, Y., Shi, L., Zhu, Y., 2007. Solid-phase photocatalytic degradation of polyethylene plastic under UV and solar light irradiation. J. Mol. Catal. Chem. 268 (1–2), 101–106.
Zhu, D., Bi, Q., Xiang, Q., Chen, Q., Christie, P., Ke, X., Wu, L., Zhu, Y., 2018. Trophic predator-prey relationships promote transport of microplastics compared with the single *Hypoaspis aculeifer* and *folsomia candida*. Environmental Pollution 235, 150–154. https://doi.org/10.1016/j.envpol.2017.12.058.

Update

Journal of Environmental Management

Volume 404, Issue , 15 April 2026, Page

DOI: https://doi.org/10.1016/j.jenvman.2026.129332

Journal of Environmental Management 404 (2026) 129332

Contents lists available at ScienceDirect

Journal of Environmental Management

journal homepage: www.elsevier.com/locate/jenvman

Corrigendum to "Advanced TiO_2-based catalysts for polypropylene degradation in aquatic media" [J. Environ. Manag. 394 (2025) 127289]

A. Egea-Corbacho [a,b], A.P. Martín-García [a,*], J.M. Salas-Calvo [a], D. Coello [a,b], R. Rodríguez [a,c], I. Moreno-Garrido [d], M. Sendra [d], M.P. Yeste [e,f]

[a] Department of Environmental Technologies, Faculty of Marine and Environmental Sciences, University of Cadiz, Puerto Real, 11510, Cádiz, Spain
[b] INMAR-Marine Research Institute, CEIMAR International Campus of Excellence of the Sea, University of Cadiz, Puerto Real, Cadiz, Spain
[c] IVAGRO-Wine and Agrifood Research Institute, University of Cadiz, Puerto Real, 11510, Cádiz, Spain
[d] Department of Ecology and Coastal Management, Institute of Marine Sciences of Andalusia (ICMAN-CSIC), Campus Río San Pedro, Puerto Real, 11510, Cádiz, Spain
[e] Department of Materials Science and Metallurgical Engineering and Inorganic Chemistry, Universidad de Cádiz, Puerto Real, 11510, Spain
[f] Instituto de Microscopía Electrónica y Materiales (IMEYMAT), Universidad de Cadiz, Puerto Real, 11510, Spain

The authors regret the typographical error detected in Table 7, entitled "Table 7. Ce, Zn and Ti concentrations applied by ICP technique." The title of the table is correct, as are the data presented. However, the header of the table was misplaced: where it currently reads "Zn Ti Ce" it should instead read "Ce Zn Ti" in order to correctly align with the values shown.

This error has also been carried into the text, where "Ti" is repeated twice in the following sentence: "However, as for Ti, there is an appreciable concentration in the catalysts formed by ZnO/TiO_2 and $ZnO\text{-}CeO_2/TiO_2$." This should be corrected to: "However, as for Zn, there is an appreciable concentration in the catalysts formed by ZnO/TiO_2 and $ZnO\text{-}CeO_2/TiO_2$."

In the Highlights section, where it currently states: "Ti leaching was detected in water after photocatalytic activity, which must be further studied." This should be corrected to: "Zn leaching was detected in water after photocatalytic activity, which must be further studied."

The authors would like to apologise for any inconvenience caused.

DOI of original article: https://doi.org/10.1016/j.jenvman.2025.127289.
* Corresponding author.
E-mail address: ana.martingarcia@uca.es (A.P. Martín-García).

https://doi.org/10.1016/j.jenvman.2026.129332

Available online 14 March 2026